Programming Research Group

A MODEL OF THE PERIPHERAL NERVOUS SYSTEM

Bryan S. Todd

PRG-TR-4-93

Oxford University Computing Laboratory
Wolfson Building, Parks Road, Oxford OX1 3QD

A Model of the Peripheral Nervous System

Bryan S. Todd

Abstract

A simple model of the peripheral nervous system of the human upper limb is presented. The model is a refinement of an earlier model that forms part of a diagnostic program to assist the localization of nerve lesions. The purpose of this work is both to simplify the mathematical description of the model, and to extend the model to include a more detailed representation of the distribution of nerve fibres. The numerical parameters in the model are derived from published experimental data by least-squares optimization, and the model is validated by comparison with further experimental data.

Introduction

Localization of lesions of the peripheral nervous system from their clinical manifestations entails anatomical reasoning. The relevant anatomy is well-documented, and provided that only a single lesion is present, the task is usually straightforward. Several explanatory guides to the localization of nerve lesions can be found in the medical literature [Sun78, Swa86, Mil87]. However, when multiple lesions are present the task is more difficult, and clinical accuracy falls. This has motivated the development of several computer programs to provide assistance in more complicated cases.

The earliest program appears to be due to First *et al* [Fir82]. This program ('LOCALIZE') incorporates a detailed model of anatomy, with 2,244 named nervous system structures. Possible minimal sets of lesions are postulated which are consistent with all observations. However, since logical reasoning rather than statistical inference is employed, the number of alternative solutions can be large if observer error or anatomical variation causes an inconsistency. The system's diagnostic accuracy does not appear to have been fully evaluated. By contrast, the 'PLEXUS' program [Jas87] copes with uncertainty in observation. However, medical knowledge was originally represented in the form of inference rules, although Reggia [Reg78] had earlier reported difficulty with this representation for the central nervous system and greater success had been achieved with explicit anatomical models [Cat79]. A model of the peripheral nervous system was subsequently introduced into the PLEXUS system. When tested on 15 unseen cases, the system's diagnostic conclusions were judged to be 'good' in 12 cases, and 'fair' in the other three [Jas90]. Information about nerve pathways is also included in the similarly named 'PLEXXUS' program [Fis90]. Like LOCALIZE, PLEXXUS searches for a single lesion that explains all findings. If this fails, as may happen when multiple lesions are present, PLEXXUS displays the proportion of abnormal findings each possible lesion can explain, and thus gives some indication of the relative likelihood of lesions. The accuracy of the system on difficult cases is, however, unclear.

An alternative approach has been taken at the Programming Research Group; we have developed a probabilistic simulation model of the peripheral nervous system of the upper limb [Tod87, Hai88]. This reflects a general trend in expert system research away from rule-based representations and unsound calculi of uncertainty, towards probabilistic causal representations [Nea89, And91]. Our model includes an explicit description of the nerve pathways, and of the actions of various muscles. This allows prediction of the expected clinical manifestations given any pattern of nerve injury. The model also specifies the probability of observations deviating from those expected. The main weakness of the model, however, is an assumption that lesions occur independently of one another, whereas experience suggests that statistical dependencies exist [Tod88]. Nevertheless, despite this, the program was found to be significantly more accurate than three clinicians with whom it was compared on 26 cases [Tod90, Bur91]. The motivation for the present study was to try to weaken the independence assumption by predicting commoner patterns of injury using the anatomical information in the model. Slightly more detailed anatomical information about the distribution of nerve fibres is required for this than is provided by the original model. This paper presents only a revised model of the nerve anatomy; the question of predicting clusters of lesions is not addressed here. Paradoxically, the refined model has a simpler mathematical description than before [Tod88].

The model specifies the distribution of the nerve fibres emanating from the spinal cord to supply the upper limb. At each branching point in the peripheral nervous system, the proportion of fibres following each of the possible courses is specified explicitly. This means that both the cross-sectional areas of individual nerves, and the root contribution to each muscle can be calculated. These predictions are compared to actual measurements of nerves, and to the myotomes described in the original model which were based on accounts given in standard textbooks. The style of presentation of the model is top-down refinement; initially the anatomy is described as a collections of pathways and later it is shown how to represent these as trees. The notation and conventions of the Z specification language are adopted in the formal section because they have been fully documented elsewhere [Spi88].

Model Design

More than a hundred thousand nerve fibres emanate from the cervical enlargement of the spinal cord to supply the upper limb [Nar78]. The anatomical distribution of these fibres as they course distally constitutes the anatomy that is relevant to the task of localizing nerve lesions. Each nerve fibre follows a particular pathway eventually reaching a muscle or sensory area, which it innervates. Mathematically, the distinction between a muscle and a sensory area is irrelevant from the point of view of localizing nerve lesions. We therefore drop the distinction and instead refer to both as 'end-organs'. The entire distribution of the fibres leaving the cervical enlargement of the spinal cord is thus described by the proportion which follow each pathway to each end-organ.

$$\mathrm{NerveAnatomy} \;\widehat{=}\; \mathbb{D}\,(\mathrm{Pathway} \times \mathrm{EndOrgan}) \tag{1}$$

Here the symbol $\mathbb{D}$ denotes construction of all proportional distributions over its argument. Formally, for any countable set T,

$$\mathbb{D}T \;\widehat{=}\; \{d : T \rightarrow \mathbb{R}^+ \;\mid\; \sum_{t:T} d(t) = 1\} \tag{2}$$

where $\mathbb{R}^+$ denotes the set of all non-negative real numbers.

A fibre follows a pathway which consists of a sequence of named nerves, or segments of nerves.

$$\mathrm{Pathway} \;\widehat{=}\; \mathsf{seq}\,\mathrm{Nerve} \tag{3}$$

It is assumed that individual fibres do not branch; although there is evidence that branching *does* occur [Sun78] it does not appear to be of clinical significance.

Since the purpose of the model is to assist the localization of lesions from their clinical manifestations, we consider only fibres supplying muscles or cutaneous sensory receptors. We ignore, for example, autonomic and proprioceptive fibres. A sensory end-organ thus consists of a collection of cutaneous sensory receptors. Since some dermatomes (C6 for example) extend over a large area, yet are supplied by more than one cutaneous nerve, we subdivide each such dermatome into several sensory end-organs, one for each corresponding cutaneous nerve. Thus in our model, C6 dermatome is composed of three sensory end-organs which we refer to as sensory organs C6-1, C6-2 and C6-3. These are supplied by the palmar cutaneous branch of the median nerve, the palmar digital branch(es) of the median nerve, and the superficial branch of the radial nerve in the forearm, respectively.

Some Examples

Our model contains 51 nerves involved in the supply to the upper limb. The following is an example of a nerve pathway.

$$P \mathrel{\widehat{=}} \langle \ \text{C5\_root}, \ \ \text{upper\_trunk}, \ \ \text{suprascapular\_nerve} \ \rangle$$

According to our model, 1.30% of fibres follow pathway P to infraspinatus. Therefore, if N is the nerve anatomy described by the model,

$$N(P, \text{infraspinatus}) = 0.0130$$

However, no fibres reach brachialis by this route. Thus,

$$N(P, \text{brachialis}) = 0$$

Similarly, $N(p, e) = 0$ for any pathway p and end-organ e such that p is either anatomically impossible, or p does not lead to e, or p does not reach e.

Some Functions

The anatomical model allows us to calculate several parameters. Let N denote the model, and let n denote an arbitrary nerve. We define the *size* of n (denoted $\mathcal{S}(N)(n)$) to be the proportion of fibres which travel through n. This is calculated by summing the proportions of fibres which supply any end-organ via a pathway on which n lies.

$$\begin{aligned} &\mathcal{S} : \text{NerveAnatomy} \to \text{Nerve} \to \mathbb{R}^+ \\ &\forall N : \text{NerveAnatomy} \bullet \\ &\qquad \mathcal{S}(N) = \lambda n : \text{Nerve} \bullet \sum_{p:\text{Pathway};e:\text{EndOrgan} \mid n \in \operatorname{ran} p} N(p, e) \end{aligned} \tag{4}$$

For example, according to our model N, approximately 32.09% of the fibres emanating from the cervical enlargement of the spinal cord pass through the upper trunk. Thus,

$$\mathcal{S}(N)(\text{upper\_trunk}) = 0.3209$$

Provided that no fibres loop back to pass through the same nerve more than once (this does not happen in practice), $\mathcal{S}(N)(n)$ is proportional to the number of fibres which comprise nerve n.

This concept extends to end-organs too. Here 'size' refers not to the physical size of the end-organ, but to the relative number of fibres which innervate the end-organ. The definition is slightly simpler.

$$\begin{aligned}
&\mathcal{S} : \text{NerveAnatomy} \rightarrow \text{EndOrgan} \rightarrow \mathbb{R}^+ \\
&\forall N : \text{NerveAnatomy} \bullet \\
&\qquad \mathcal{S}(N) = \lambda e : \text{EndOrgan} \bullet \sum_{p:\text{Pathway}} N(p, e)
\end{aligned} \tag{5}$$

For example, according to our model N, approximately 6.46% of the fibres emanating from the cervical enlargement of the spinal cord supply triceps. Thus,

$$\mathcal{S}(N)(\text{triceps}) = 0.0646$$

We can also condition the above parameter on the requirement that the fibres travel through a specified nerve.

$$\begin{aligned}
&\mathcal{S} : \text{NerveAnatomy} \rightarrow \text{EndOrgan} \rightarrow \text{Nerve} \rightarrow \mathbb{R}^+ \\
&\forall N : \text{NerveAnatomy} \bullet \\
&\qquad \mathcal{S}(N) = \lambda e : \text{EndOrgan} \bullet \lambda n : \text{Nerve} \bullet \sum_{p:\text{Pathway} \,|\, n \in \operatorname{ran} p} N(p, e)
\end{aligned} \tag{6}$$

For example, according to our model N, approximately 2.20% of the fibres emanating from the cervical enlargement of the spinal cord supply triceps via a pathway including the C7 spinal root. Thus,

$$\mathcal{S}(N)(\text{triceps})(\text{C7\_root}) = 0.0220$$

Therefore the proportion of the supply to triceps representing C7 fibres is 0.34 ($\approx 0.0220/0.0646$). Thus we can calculate myotomes from the model.

Nerve Trees

Explicit enumeration of pathways is a cumbersome method of representing nerve anatomy. It is more efficient to represent the distribution of fibres as a tree. This is how the nerve anatomy was represented in our original model, and how, for example, it is represented in 'NERVTRACK', a computerized database of neurological anatomy [Spi89]. The difference here is that we include numerical information at each node of the tree to indicate the relative proportion of fibres which follow each alternative course. A tree is defined recursively. It is either an end-organ, or a nerve leading to finite set of trees, each associated with a parameter specifying the proportion of fibres in the nerve which enter that tree.

$$\text{Tree} ::= \text{eo}\langle\langle \text{EndOrgan} \rangle\rangle \mid \text{nv}\langle\langle \text{Nerve} \times \mathbb{D}^{\text{F}}\,\text{Tree} \rangle\rangle \tag{7}$$

Here the symbol $\mathbb{D}^{\text{F}}$ denotes the construction of a finite distribution over its argument. Formally, for any set T,

$$\mathbb{D}^{\text{F}} T \;\widehat{=}\; \{ d : T \twoheadrightarrow\!\!\!\!\!\!\;\;\mapsto \mathbb{R}^+ \mid \sum_{t:\operatorname{dom} d} d(t) = 1 \} \tag{8}$$

In the original model, nerve trees contained no numerical information; the root contributions to each end-organ were described separately [Tod88]. However, this led to awkward consistency requirements between the two components. These difficulties are avoided here by including the numerical information within the tree itself.

Since fibres leave the spinal cord through various root nerves, no single tree represents the course of these fibres. Instead we represent the anatomy as a finite distribution over trees, one for each spinal root.

$$\text{Trees} \;\widehat{=}\; \mathbb{D}^{\mathrm{F}}\,\text{Tree} \tag{9}$$

The explicit anatomy is easily recovered from the tree representation.

$$\mathcal{A} : \text{Trees} \rightarrow \text{NerveAnatomy} \tag{10}$$

$$\forall d : \text{Trees}; e : \text{EndOrgan}; n : \text{Nerve}; p : \text{Pathway} \bullet$$

$$\begin{aligned}
\mathcal{A}(d)(\langle\rangle, e) &= \begin{cases} 0 & \text{eo}(e) \notin \mathsf{dom}\, d \\ d(\text{eo}(e)) & \text{eo}(e) \in \mathsf{dom}\, d \end{cases} \\
\mathcal{A}(d)(\langle n \rangle \frown p, e) &= \sum_{d' : \text{Trees} \,\mid\, \text{nv}(n, d') \in \mathsf{dom}\, d} d(\text{nv}(n, d')) \times \mathcal{A}(d')(p, e)
\end{aligned}$$

Model Construction

In constructing trees of fibre distributions, we adapted the trees in the original model. We have made three significant alterations.

1. The C4 and T2 roots have been omitted. These were originally included in the model only to represent preservation of partial sensation in the C5 and T1 dermatomes after denervation of C5 and T1, owing to dermatomal overlap. However, the possibility of lesions of the C4 and T2 roots were never entertained, and so there is no need to represent these two roots explicitly in the model. Instead, fibres are now considered to travel directly from the spinal cord to the C4 and T2 sensory end-organs without passing through any nerves.
2. The musculocutaneous nerves in the axilla and the arm have been combined into a single segment 'musculocutaneous nerve in the axilla/arm' because only the contractility of coracobrachialis helps to distinguish the level of the lesion, and this is too unreliable a sign to enable much discrimination.
3. Both heads of the median nerve have been introduced into the model, since selective lesions of either do occur, and can be localized clinically.

The new model is shown in the appendix.

Numerical Parameters

The numerical parameters for the original model were subjective estimates of myotomal and dermatomal distributions based on qualitative accounts in the literature. Although fully comprehensive descriptions of the microscopic anatomy of the peripheral nervous system have never been compiled, some data for the brachial plexus are now available, and these complement earlier studies of more peripheral nerves. Therefore we elected to calculate the numerical parameters for the model entirely from published data.

The one of the most detailed and accurate studies of the microscopic anatomy of the human brachial plexus is that of Slingluff et al [Sli87]. This entailed computer-aided measurement of the neural content of approximately 20,000 sections of the brachial plexus. Measurements from seven different cadavers provide reliable estimates of the neural cross-sectional areas of 27 components of the brachial plexus. The means and variances of the estimates are summarized in Table 1 (Page 7). The data are displayed to a few decimal places, although all calculations were performed with the maximum available precision. The source of most of these data are Tables 22-8 and 22-9 of Slingluff et al [Sli87], with the following qualifications and exceptions.

1. Where two branches of the lateral pectoral nerve were present, the areas of the two branches were combined before taking the average of the seven specimens.
2. The sizes of the subscapular and axillary nerves are difficult to assess from the data given in Table 22-9 because the two nerves are combined in two of the seven specimens. Therefore the separate estimates given in Table 22-10 are used instead. The size of the axillary nerve is taken as the sum of the sizes of the motor and sensory components. Furthermore, the sensory component itself is assumed to correspond to the upper lateral brachial cutaneous nerve.
3. The intercostobrachial nerve is assumed to represent the T2 contribution to the plexus.

Except for four nerves, the variance of the estimate of the population mean was calculated according to

$$\text{variance} = \frac{\sum_{1 \le i \le n} (\text{observation}_i - \text{mean})^2}{n(n-1)} \tag{11}$$

where n is the number of specimens in which the nerve was measured. The four exceptions were the medial brachial cutaneous nerve, the subscapular nerve, the axillary nerve, and the upper lateral brachial cutaneous nerve. The above formula could not be used for these four nerves as the medial brachial cutaneous nerve was observed in only one specimen, and in the case of the other three, only the mean values were published. Therefore, noting a close correlation between the mean and the standard deviation of the estimate, linear interpolation was used. For each of the other 23 nerves in turn the standard deviation was divided by the mean. The average of these 23 fractions was then taken to be the constant of proportionality for the dependence of standard deviation on mean area for the other four nerves.

Our task is to determine from these data the relative number of fibres following each pathway to each end-organ. There are 101 such pathway–end-organ pairs in the nerve tree. We index these from 0 to 100. For each j $(0 \le j \le 100)$, p_j is the pathway, e_j is the end-organ, and x_j is the cross-sectional area (mm^2) of neural tissue comprised of fibres following p_j to e_j. We assume that the number of fibres comprising any given pathway is directly proportional to the cross-sectional area of the neural tissue; Slingluff et al reported a close correspondence between their measurements of neural tissue area and axon counts [Sli87].

Due to observational error and anatomical variation, the data shown in Table 1 are not entirely compatible. For example, the sum of the areas of the C5 and C6 roots is 10.59mm^2, yet the sum of the areas of the upper trunk, suprascapular nerve and dorsal scapular nerve is 11.15mm^2. This inequality is even more marked if one makes allowance for a contribution from C5 and C6 to the long thoracic nerve. Therefore, we calculate the sizes of the pathways by means of least-squares optimization. Table 1 gives rise to 27 linear equations $(0 \le i \le 26)$ of the form

$$\sum_{0 \le j \le 100} a_{ij} x_j = b_i \tag{12}$$

where a_{ij} is one or zero according to whether or not the i^{th} nerve lies on pathway p_j, and b_i is the observed area of neural tissue in mm^2. Following the usual least-squares procedure, the weight w_i assigned to each such equation is the reciprocal of the variance of the observation b_i.

Table 1: Total cross-sectional area (mm^2) of neural tissue in 27 nerves. The table shows the mean and variance of each estimate, and the weight assigned each observational equation (see text). Source of data: Slingluff et al [Sli87].

Nerve	No. Specimens	Mean Area (b_i)	Variance	Weight (w_i)
C5 root	7	3.80	0.2788	3.59
C6 root	7	6.79	0.1120	8.93
C7 root	7	6.89	0.2044	4.89
C8 root	7	6.74	0.4090	2.45
T1 root	7	4.33	0.3851	2.60
T2 root	3	0.19	0.0010	1012.04
Dorsal scapular nerve	6	0.35	0.0029	342.71
Long thoracic nerve	7	0.83	0.0053	187.83
Upper trunk of the brachial plexus	7	9.55	0.5153	1.94
Middle trunk of the brachial plexus	7	6.85	0.2028	4.93
Lower trunk of the brachial plexus	7	10.44	0.9843	1.02
Suprascapular nerve	7	1.25	0.0095	105.54
Lateral cord of the brachial plexus	7	6.97	0.4701	2.13
Medial cord of the brachial plexus	7	7.37	1.0785	0.93
Posterior cord of the brachial plexus	7	9.47	0.4039	2.48
Lateral pectoral nerve	7	1.20	0.0088	113.50
Medial pectoral nerve	6	0.37	0.0285	35.12
Medial brachial cutaneous nerve	1	0.19	0.0005	2196.80
Medial antebrachial cutaneous nerve	7	1.04	0.0105	95.10
Thoracodorsal nerve	5	0.60	0.0042	238.64
Subscapular nerve	1	1.07	0.0153	65.33
Musculocutaneous nerve (in axilla/arm)	7	1.91	0.1026	9.75
Median nerve (in axilla/arm)	7	5.86	0.2133	4.69
Ulnar nerve (in axilla/arm)	7	3.77	0.0791	12.64
Axillary nerve	1	2.22	0.0656	15.24
Upper lateral brachial cutaneous nerve	1	0.42	0.0023	437.34
Radial nerve (in axilla)	7	5.54	0.1222	8.18

The number of equations (27) is less than the number of unknowns (101). Therefore, the pathway sizes are underdetermined. However, further information is given about the more distal branches of the nerve trunks by an earlier study by Sunderland and Bedbrook [Sun49]. The measurements of particular importance concern the proportion of cutaneous sensory fibres in the radial, median and ulnar nerves. The data are shown in Table 2 (Page 8). The variance was calculated according to Equation 11.

Table 2 gives rise to three further observational equations of the form of Equation 12 ($27 \leq i \leq 29$). For each of these three equations, b_i is zero, and a_{ij} is given by

$$a_{ij} = \begin{cases} 0 & \text{The nerve does not lie on the pathway.} \\ m_i - 1 & \text{The nerve lies on the pathway, and the end-organ is sensory.} \\ m_i & \text{The nerve lies on the pathway, and the end-organ is motor.} \end{cases}$$

where m_i is the mean proportion of the neural cross-sectional area comprised of sensory fibres. The weight of each of the three equations is given by the reciprocal of the variance of the sensory fibre area. Since only variances of proportions are given, these were first multiplied by the square of the total

Table 2: Proportions of cross-sectional area of neural tissue comprised of cutaneous fibres in three nerves. Source of data: Sunderland and Bedbrook [Sun49].

Nerve	No. Specimens	Mean Proportion (m_i)	Variance	Weight (w_i)
Radial nerve (in arm)	11	0.2891	0.0001845	705.74
Median nerve (in axilla/arm)	10	0.6710	0.0001610	180.81
Ulnar nerve (in axilla/arm)	12	0.5442	0.0001734	406.04

areas of neural tissue as given in Table 1. Thus

$$\text{weight} = \frac{1}{\text{area}^2 \times \text{variance}}$$

Table 1 provides no direct observations of the radial nerve in the arm, so for the purpose of calculating the weight of importance, the area was taken to be half that of the radial nerve in the axilla. (This was confirmed by independent measurements of the two nerves in dissected specimens — see later.)

The total number of equations (30) is still considerably less than the number of unknowns (101). Therefore we make a default assumption that, in the absence of evidence to the contrary, all pathway–end-organ pairs are of equal size. The total size of the C5 to T1 roots inclusive is 28.5360mm^2 [Sli87]. These comprise 99 distinct pathways to end-organs in our model. (The other two are from C4 and T2, respectively.) This gives a default value of 0.288242mm^2 ($\approx 28.5360 \div 99$) for each x_j. Thus we have 101 further observational equations of the form

$$x_j = 0.288242 \tag{13}$$

Initial experiments with least-squares optimization soon confirmed a tendency for some pathways to assume negative values. Therefore we bounded pathways to positive sizes by replacing the 101 default equations (Equation 13) with their logarithmic form

$$\ln x_j = -1.243955 \tag{14}$$

These default equations we assign a weight (10^{-3}) small enough so that they have negligible effect if actual observations provide evidence about the size of the respective pathways, yet not so small as to be lost in rounding error due to limited real number precision. An iterative optimization algorithm is required as these equations are non-linear. We initialize the unknowns x_j to their default value (0.288242), and then at each iteration we solve for the change (Δx_j) in each x_j required to minimize the weighted residuals. This entails a least-squares optimization of 101 unknowns (Δx_j) to minimize the weighted residuals of 131 observational equations. The first 30 equations have the form

$$\sum_{0 \le j \le 100} a_{ij} \Delta x_j = b_i - \sum_{0 \le j \le 100} a_{ij} x_j \tag{15}$$

The remaining 101 equations (obtained by differentiating Equation 14) have the form

$$\frac{\Delta x_j}{x_j} = -1.243955 - \ln x_j \tag{16}$$

At the end of each iteration, we update the x_j according to

$$x_j := x_j + \frac{\Delta x_j}{3}$$

Inclusion of only one third the calculated difference makes the optimization procedure stable. The stopping criterion is that the largest absolute size of any Δx_j should be less than 10^{-4}. This requires 28 iterations. The error E that this minimizes is given by

$$E \hat{=} \sum_{0\leq i\leq 29} w_i \left(b_i - \sum_{0\leq j\leq 100} a_{ij} x_j \right)^2 + \sum_{0\leq j\leq 100} 10^{-3} (\ln x_j + 1.243955)^2 \qquad (17)$$

where the w_i are the weights shown in Tables 1 and 2.

The nerve anatomy N is then obtained by normalization. For each j,

$$N(p_j, e_j) = \frac{x_j}{\sum_{0\leq k\leq 100} x_k} \qquad (18)$$

and all other pairs map to zero. Simultaneously, the denominator in the above equation represents the total cross-sectional area (28.74mm^2) of neural tissue emanating from the cervical enlargement of the spinal cord that is represented in the model.

Having obtained N in this way, we calculated the numerical parameters of the nerve trees. As a final step we rounded the parameters to two decimal places as shown in the appendix. This is now the final form of the model (rounding of the parameters means that it specifies a slightly different N). The modelling assumptions that have been made are

1. Nerve fibres do not branch within the peripheral nervous system.
2. The anatomy of the peripheral nervous system is constant and does not vary between individuals.
3. The pathways shown in the nerve trees in the appendix are a complete and correct representation of the pathways that actually exist.
4. The total number of motor and cutaneous sensory fibres in a nerve is directly proportional to the cross-sectional area of neural tissue.

Model Validation

In validating the model we can examine first the correspondence achieved between actual observations and predictions. However, a stronger validation requires access to further observations, not used in the optimization procedure. For this purpose, we collected our own data. Four cadaver specimens that had been previously dissected were examined. In each case, the upper limb in which the peripheral nervous system was best displayed was selected for measurements. Only if a nerve could not be clearly identified in this limb was the corresponding nerve sought and measured if possible in the opposite limb. Measurements were taken by eye using a ruler; the largest and smallest diameters of each nerve were recorded in millimetres. Table 3 (Page 16) shows the figures obtained.

Cross-sectional areas were calculated from these measurements on the assumption that a transverse section through the nerve forms a perfect ellipse (area $= \pi \times \text{radius}_{\text{max}} \times \text{radius}_{\text{min}}$). In Cadaver 2 the middle trunk was found to be fused with the lower trunk which was consequently very wide (14mm by 5mm) with a cross-sectional area of 54.98mm^2. (We are working to more significant figures than can be supported by the accuracy of the measurements in order to avoid rounding errors.) Therefore, since we are interested in the measurements of the normal brachial plexus, rather than its variations, the idealized sizes of the middle and lower trunks of Cadaver 2 were estimated. This was carried out by extrapolation from the other two specimens in which both the lower and middle trunks were measured (Cadavers 2 and 3). In those two specimens, the cross-sectional area of the middle trunk represented respectively 41.67% and 28.01% of the total area of both middle and lower trunks. The average of these two proportions is 34.84%. The idealized cross-sectional area of the middle trunk of Cadaver 2 was thus estimated to be 19.16mm^2 (= 54.98×0.3484), and the corresponding area for the lower trunk was reduced to 35.82mm^2 (= $54.98 - 19.16$). Similar extrapolations were carried out for the middle anterior, middle posterior, lower anterior and lower posterior divisions. In the case of the posterior divisions, extrapolation could be made only from Cadaver 3 as the size of the lower posterior division had not been measured in either Cadaver 1 or Cadaver 4. The calculated areas are shown in Table 4 (Page 17).

Inspection of Table 4 shows a reasonable correlation of the cross-sectional areas of nerves between the four specimens. In a few instances, wide differences are observed. For example, the cross-sectional area of the upper posterior division varies from 4.12mm^2 (Cadaver 2) to 15.71mm^2 (Cadaver 4). Nevertheless, this is attributable to natural variation; the anatomy of the brachial plexus is known to vary significantly from the norm in about 10% of persons. Furthermore, the measurements given are consistent with those reported in the literature. In a study of 24 specimens [Sun61], measurements made by Sunderland and Bradley show the mean cross-sectional area of the median and ulnar nerves to be 9.44mm^2 (standard deviation 2.25mm^2) and 7.27mm^2 (standard deviation 1.48mm^2), respectively. These compare favourably with our estimates of 9.23mm^2 and 6.28mm^2. Furthermore, the minimum and maximum cross-sectional areas of four other nerves were reported. These are shown in Table 5 (Page 18) and compared with our estimates. Comparison with those of Slingluff et al (Table 1) is complicated by the fact that our estimates are of total cross-sectional area while Slingluff et al measured the cross-sectional area of neural tissue alone. However, they reported that on average neural tissue comprised one third of the total cross-sectional area [Sli87]. If we divide our estimates by 3, we obtain a reasonable correspondence with those in Table 1 too. The main discrepancies are that our estimates of the C5 and C6 spinal roots are too small (1.83mm^2 and 3.84mm^2 compared to 3.80mm^2 and 6.79mm^2, respectively), and our estimate of the medial brachial cutaneous nerve is too large (1.18mm^2 compared to 0.19mm^2). Access to the spinal roots was difficult, however, and so measurements are unreliable, even in the two specimens in which it proved possible. The large discrepancy in the case of the medial brachial cutaneous nerve could be partly explained if the neural content were less than average; Slingluff et al report that the neural content of the medial antebrachial cutaneous nerve is 0.156, less than half the average for all nerves.

Table 6 (Page 19) compares predictions with observations of the cross-sectional area of neural tissue in each nerve. The second column lists the areas of neural tissue as predicted by the model shown in the appendix. The sizes have been scaled by a factor of 28.74 (the denominator of Equation 18) in order to convert proportions to absolute sizes in mm^2. The third column reproduces the estimates of Slingluff et al (Table 1), for comparison. The fourth column shows our own measurements (Table 4), divided by 3 in order to convert estimates of total cross-sectional area to those of just neural tissue. These data are shown graphically on a logarithmic scale in Figure 1 (Page 11). The most notable differences that have not already been discussed are that our estimates for the median and ulnar nerves are generally too small. To some extent this may be explained by drying out of the more peripheral nerves in the cadavers. Another additional explanation is that the median and ulnar nerves have less connective tissue than average; Slingluff et al report that the proportion of neural tissue for the median and ulnar nerves is 0.435 and 0.431, respectively [Sli87].

The model predicts the lower posterior division to be very small indeed (cross-sectional area of neural tissue 1.98mm^2) while the lower anterior division is quite large (7.34mm^2). Although an inequality in this direction was actually observed, it was much smaller (3.73mm^2 and 4.36mm^2). However, following the methods of early anatomists, Narakas has drawn maps based on microscopic dissections of several fresh human cadavers [Nar78, Nar81]. These diagrams show that only about a third of fibres in C8 spinal root pass posteriorly, the rest pass anteriorly to join T1 fibres in the lower trunk [Nar78, Nar81]. This compares favourably with our model (see the appendix); according to our model, 30% of C8 fibres pass posteriorly and 70% pass anteriorly. In Narakas' diagrams, the lower posterior division is shown to be much smaller than the lower anterior division, and is the smallest of the three posterior divisions. Similar proportions are seen in Kerr's diagrams [Ker18]. Harris also points out that the posterior divisions of the upper nerves are larger than that of C8 [Har39].

Figure 1: Graph displaying the data from Table 6. The logarithm of predicted cross-sectional area (mm^2) is plotted against the logarithm of observed cross-sectional area (mm^2) for all nerves in which observations are available. The data from Slingluff et al are shown as shaded circles, and our data are shown as unshaded circles.

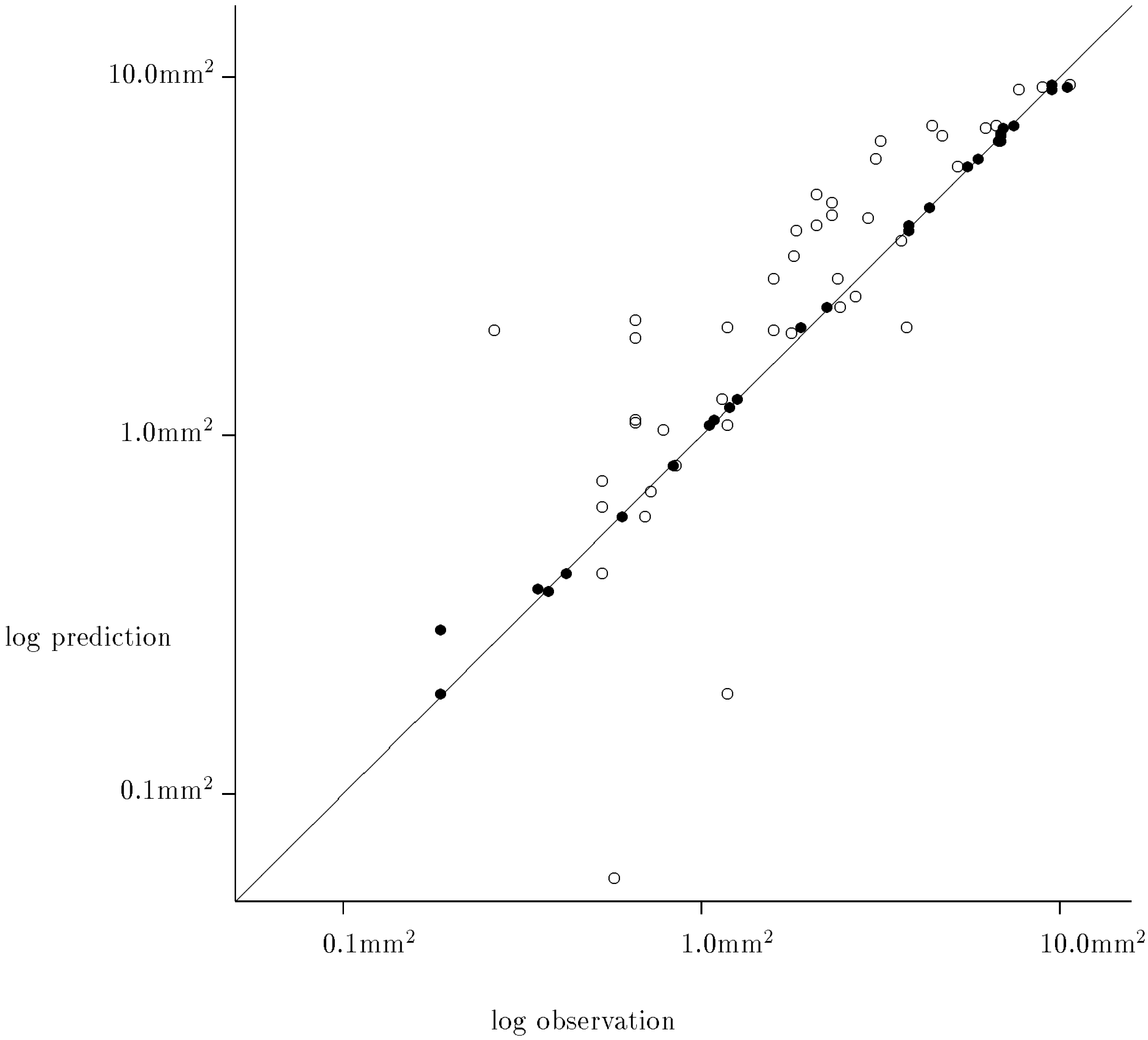

The equations arising from the data concerning the proportion of cutaneous sensory fibres in three nerves (Table 2) were assigned high weights. Consequently a close fit to the data was obtained (Table 7, Page 20).

Myotomes

A further experiment is to calculate myotomes from the model, and compare these with the myotomes described in standard textbooks. The latter were given a subjective numerical interpretation and used in the original model. However, they are reproduced qualitatively in Table 8 (Page 20) and compared with the model predictions. In many cases where there appears to be a discrepancy, the standard is itself open to question. For example, accumulated clinical experience suggests that latissimus dorsi, extensor carpi ulnaris, extensor pollicis longus, extensor pollicis brevis, and abductor pollicis longus are indeed innervated mainly by C7 [MRC76]. However, in other cases there seems to be genuine error. For example, the model predicts that subscapularis and teres major are innervated mainly by C7, yet this is not consistent with the calculations carried out by Slingluff et al [Sli87] which suggest that most of the supply is via the upper trunk (the conventional view is that C6 is mainly responsible). Similarly the model places more emphasis on C8 than on T1 for the innervation of the interossei, and this seems wrong. Correspondence on the whole, however, is reasonable.

Conclusion

Although there are still some discrepancies between predictions and observations, this study has shown that the model of the peripheral nervous system can be extended to include more detailed information about the distribution of fibres than before, and still retain a reasonable approximation to observable anatomical parameters. Moreover, the numerical parameters appearing in the model have been derived by objective means from actual observations. Clearly further work needs to be done to determine the microscopic anatomy of the peripheral nervous system more precisely. As further results become available, these will need to be incorporated into our calculations so that the model become an ever more faithful representation of the true anatomy.

Appendix

Shown below are the distribution trees for fibres leaving the cervical enlargement of the spinal cord. An indented depth-first format is used, so that common children of a node are left-aligned vertically. The root node of each sub-tree is preceded on the same line by the proportion of fibres from the parent node which enter that sub-tree.

- 0.01 Sensory organ C4
- 0.13 C5 root
  - 0.10 Dorsal scapular nerve
    - 1.00 Rhomboids
  - 0.13 Long thoracic nerve
    - 1.00 Serratus anterior
  - 0.77 Upper trunk of the brachial plexus
    - 0.26 Suprascapular nerve
      - 0.50 Supraspinatus
      - 0.50 Infraspinatus
    - 0.10 Upper anterior division of brachial plexus
      - 1.00 Lateral cord of the brachial plexus
        - 0.20 Lateral pectoral nerve
          - 1.00 Pectoralis major
        - 0.80 Musculocutaneous nerve (in axilla/arm)
          - 0.25 Coracobrachialis
          - 0.25 Biceps brachii
          - 0.25 Brachialis
          - 0.25 Lateral antebrachial cutaneous nerve
            - 1.00 Sensory organ C5-3
    - 0.64 Upper posterior division of brachial plexus
      - 1.00 Posterior cord of the brachial plexus
        - 0.03 Subscapular nerve
          - 1.00 Subscapularis
        - 0.89 Axillary nerve
          - 0.38 Deltoid
          - 0.37 Teres minor
          - 0.25 Upper lateral brachial cutaneous nerve
            - 1.00 Sensory organ C5-1
        - 0.08 Radial nerve (in axilla)
          - 0.39 Lower lateral brachial cutaneous nerve
            - 1.00 Sensory organ C5-2
          - 0.61 Radial nerve (in arm)
            - 0.50 Brachioradialis
            - 0.50 Posterior interosseous nerve
              - 1.00 Supinator
- 0.23 C6 root
  - 0.04 Long thoracic nerve
    - 1.00 Serratus anterior
  - 0.96 Upper trunk of the brachial plexus
    - 0.08 Suprascapular nerve
      - 0.50 Supraspinatus
      - 0.50 Infraspinatus
    - 0.66 Upper anterior division of brachial plexus
      - 1.00 Lateral cord of the brachial plexus
        - 0.01 Lateral pectoral nerve
          - 1.00 Pectoralis major
        - 0.04 Musculocutaneous nerve (in axilla/arm)
          - 0.33 Coracobrachialis
          - 0.34 Biceps brachii
          - 0.33 Brachialis
        - 0.95 Lateral head of the median nerve
          - 1.00 Median nerve (in axilla/arm)
            - 0.01 Pronator teres
            - 0.01 Flexor carpi radialis
            - 0.98 Median nerve (in forearm)
              - 0.50 Palmar cutaneous branch of the median nerve
                - 1.00 Sensory organ C6-1
              - 0.50 Median nerve (in carpal tunnel)
                - 1.00 Palmar digital branches of the median nerve
                  - 1.00 Sensory organ C6-2

    - 0.26 Upper posterior division of brachial plexus
      - 1.00 Posterior cord of the brachial plexus
        - 0.03 Thoracodorsal nerve
          - 1.00 Latissimus dorsi
        - 0.06 Subscapular nerve
          - 0.50 Subscapularis
          - 0.50 Teres major
        - 0.38 Axillary nerve
          - 0.50 Deltoid
          - 0.50 Teres minor
        - 0.53 Radial nerve (in axilla)
          - 0.06 Nerve to triceps
            - 1.00 Triceps
          - 0.94 Radial nerve (in arm)
            - 0.05 Brachioradialis
            - 0.05 Extensor carpi radialis longus
            - 0.85 Radial nerve (in forearm)
              - 1.00 Sensory organ C6-3
            - 0.05 Posterior interosseous nerve
              - 1.00 Supinator
- 0.24 C7 root
  - 0.01 Long thoracic nerve
    - 1.00 Serratus anterior
  - 0.99 Middle trunk of the brachial plexus
    - 0.40 Middle anterior division of brachial plexus
      - 1.00 Lateral cord of the brachial plexus
        - 0.40 Lateral pectoral nerve
          - 1.00 Pectoralis major
        - 0.58 Musculocutaneous nerve (in axilla/arm)
          - 1.00 Coracobrachialis
        - 0.01 Lateral head of the median nerve
          - 1.00 Median nerve (in axilla/arm)
            - 0.25 Pronator teres
            - 0.25 Flexor carpi radialis
            - 0.25 Palmaris longus
            - 0.25 Flexor digitorum superficialis
        - 0.01 Ulnar nerve (in axilla/arm)
          - 1.00 Flexor carpi ulnaris
    - 0.60 Middle posterior division of brachial plexus
      - 1.00 Posterior cord of the brachial plexus
        - 0.07 Thoracodorsal nerve
          - 1.00 Latissimus dorsi
        - 0.23 Subscapular nerve
          - 0.50 Subscapularis
          - 0.50 Teres major
        - 0.70 Radial nerve (in axilla)
          - 0.22 Nerve to triceps
            - 1.00 Triceps
          - 0.22 Posterior brachial cutaneous nerve
            - 1.00 Sensory organ C7-1
          - 0.22 Posterior antebrachial cutaneous nerve
            - 1.00 Sensory organ C7-2
          - 0.34 Radial nerve (in arm)
            - 0.10 Anconeus
            - 0.10 Brachialis
            - 0.10 Brachioradialis
            - 0.10 Extensor carpi radialis longus
            - 0.10 Extensor carpi radialis brevis
            - 0.50 Posterior interosseous nerve
              - 0.20 Extensor digitorum
              - 0.20 Extensor carpi ulnaris
              - 0.20 Abductor pollicis longus
              - 0.20 Extensor pollicis longus
              - 0.20 Extensor pollicis brevis
- 0.23 C8 root
  - 1.00 Lower trunk of the brachial plexus
    - 0.70 Lower anterior division of brachial plexus
      - 1.00 Medial cord of the brachial plexus
        - 0.05 Medial pectoral nerve
          - 1.00 Pectoralis major

        - 0.28 Medial head of the median nerve
          - 1.00 Median nerve (in axilla/arm)
            - 0.11 Palmaris longus
            - 0.11 Flexor digitorum superficialis
            - 0.33 Anterior interosseous nerve
              - 0.34 Flexor digitorum profundus II + III
              - 0.33 Flexor pollicis longus
              - 0.33 Pronator quadratus
            - 0.45 Median nerve (in forearm)
              - 1.00 Median nerve (in carpal tunnel)
                - 0.25 Flexor pollicis brevis
                - 0.25 Abductor pollicis brevis
                - 0.25 Opponens pollicis
                - 0.25 Adductor pollicis
        - 0.67 Ulnar nerve (in axilla/arm)
          - 0.08 Flexor carpi ulnaris
          - 0.08 Flexor digitorum profundus IV + V
          - 0.84 Ulnar nerve (in forearm)
            - 0.80 Cutaneous branch of the ulnar nerve
              - 1.00 Sensory organ C8
            - 0.20 Deep branch of the ulnar nerve
              - 0.50 Palmar interossei
              - 0.50 Dorsal interossei
    - 0.30 Lower posterior division of brachial plexus
      - 1.00 Posterior cord of the brachial plexus
        - 0.13 Thoracodorsal nerve
          - 1.00 Latissimus dorsi
        - 0.87 Radial nerve (in axilla)
          - 0.68 Nerve to triceps
            - 1.00 Triceps
          - 0.32 Radial nerve (in arm)
            - 0.17 Extensor carpi radialis brevis
            - 0.83 Posterior interosseous nerve
              - 0.20 Extensor digitorum
              - 0.20 Extensor carpi ulnaris
              - 0.20 Abductor pollicis longus
              - 0.20 Extensor pollicis longus
              - 0.20 Extensor pollicis brevis
- 0.15 T1 root
  - 0.37 T1 pre-ganglionic sympathetic nerve
    - 1.00 Dilator pupillae
  - 0.63 Lower trunk of the brachial plexus
    - 1.00 Lower anterior division of brachial plexus
      - 1.00 Medial cord of the brachial plexus
        - 0.05 Medial pectoral nerve
          - 1.00 Pectoralis major
        - 0.07 Medial brachial cutaneous nerve
          - 1.00 Sensory organ T1-1
        - 0.39 Medial antebrachial cutaneous nerve
          - 1.00 Sensory organ T1-2
        - 0.23 Medial head of the median nerve
          - 1.00 Median nerve (in axilla/arm)
            - 0.17 Flexor digitorum superficialis
            - 0.50 Anterior interosseous nerve
              - 0.34 Flexor digitorum profundus II + III
              - 0.33 Flexor pollicis longus
              - 0.33 Pronator quadratus
            - 0.33 Median nerve (in forearm)
              - 1.00 Median nerve (in carpal tunnel)
                - 0.50 Abductor pollicis brevis
                - 0.50 Opponens pollicis
        - 0.26 Ulnar nerve (in axilla/arm)
          - 0.20 Flexor digitorum profundus IV + V
          - 0.80 Ulnar nerve (in forearm)
            - 1.00 Deep branch of the ulnar nerve
              - 0.25 Palmar interossei
              - 0.25 Dorsal interossei
              - 0.25 Adductor pollicis
              - 0.25 Flexor pollicis brevis
- 0.01 Sensory organ T2

Table 3: Maximum and minimum diameters in millimetres of each nerve segment in each of four cadavers.

Nerve	Cadaver 1	Cadaver 2	Cadaver 3	Cadaver 4
C5 root		3.0×2.0	4.0×2.0	
C6 root		4.0×2.0	8.0×2.0	
C7 root				
C8 root				
T1 root				
Dorsal scapular nerve				
Long thoracic nerve		4.0×1.0		2.5×2.0
T1 pre-ganglionic sympathetic nerve				
Upper trunk of the brachial plexus		8.0×2.5	8.0×4.0	9.0×4.0
Middle trunk of the brachial plexus			6.0×2.5	4.0×3.5
Lower trunk of the brachial plexus		14.0×5.0	7.0×3.0	9.0×4.0
Suprascapular nerve		4.0×1.0	3.0×1.5	3.0×1.5
Upper anterior division of brachial plexus		4.0×1.5	4.0×2.0	5.0×2.5
Upper posterior division of brachial plexus		3.5×1.5	4.5×3.5	5.0×4.0
Middle anterior division of brachial plexus			5.5×1.5	4.0×2.5
Middle posterior division of brachial plexus			4.0×2.5	3.0×2.5
Lower anterior division of brachial plexus		6.0×3.0	5.5×2.0	6.0×3.5
Lower posterior division of brachial plexus		7.0×2.5	5.5×2.0	
Lateral cord of the brachial plexus	6.0×4.0	9.0×3.5	6.0×2.5	6.0×4.0
Medial cord of the brachial plexus	7.0×5.5	6.0×3.0	7.0×3.5	6.5×3.0
Posterior cord of the brachial plexus	9.5×4.0	7.0×4.0		8.0×7.0
Lateral pectoral nerve				
Medial pectoral nerve				
Medial brachial cutaneous nerve	4.0×1.5	3.0×1.5		2.0×1.5
Medial antebrachial cutaneous nerve	3.0×1.5			
Thoracodorsal nerve		2.0×1.0	2.0×1.0	2.0×2.0
Subscapular nerve	3.0×1.0	2.0×1.0		
Musculocutaneous nerve (in axilla/arm)	3.0×1.5	3.0×1.5	3.0×1.5	3.0×1.5
Lateral antebrachial cutaneous nerve	3.0×1.0	1.5×1.0		2.0×1.0
Lateral head of the median nerve	4.0×2.5	6.0×3.5	5.5×1.0	4.0×2.0
Medial head of the median nerve	4.0×2.0	2.5×2.0	6.0×1.0	4.0×2.0
Median nerve (in axilla/arm)	4.0×2.5	4.0×2.0	5.0×2.5	5.5×3.0
Anterior interosseous nerve		2.0×1.0		
Median nerve (in forearm)	3.0×3.0	3.5×2.0		
Palmar cutaneous branch of the median nerve		1.0×1.0		
Median nerve (in carpal tunnel)		6.0×1.0		
Palmar digital branches of the median nerve		4.0×1.5		
Ulnar nerve (in axilla/arm)	4.0×2.5	3.5×2.0	3.5×2.0	4.0×2.0
Ulnar nerve (in forearm)	3.0×1.5	4.0×2.0		4.0×2.0
Cutaneous branch of the ulnar nerve		2.5×1.0		
Deep branch of the ulnar nerve		2.5×1.0		
Axillary nerve	5.0×2.0	4.0×3.0		3.0×2.0
Upper lateral brachial cutaneous nerve	2.0×1.0			
Radial nerve (in axilla)	7.0×2.5	6.0×3.0		8.0×3.0
Nerve to triceps	3.0×1.0	2.0×1.0		
Lower lateral brachial cutaneous nerve				
Posterior brachial cutaneous nerve		2.0×1.0		
Posterior antebrachial cutaneous nerve				
Radial nerve (in arm)	4.5×3.0	4.0×2.0	4.5×2.0	
Posterior interosseous nerve		3.0×1.0		
Radial nerve (in forearm)	2.5×1.0	2.0×1.5		

Table 4: The calculated total cross-sectional areas in mm^2 for each nerve segment in each of the four cadavers. (In the case of the lower and middle trunks and divisions of Cadaver 2 see text.)

Nerve	Cadaver 1	Cadaver 2	Cadaver 3	Cadaver 4	Mean
C5 root		4.71	6.28		5.50
C6 root		6.28	12.57		9.42
C7 root					
C8 root					
T1 root					
Dorsal scapular nerve					
Long thoracic nerve		3.14		1.96	2.55
T1 pre-ganglionic sympathetic nerve					
Upper trunk of the brachial plexus		15.71	25.13	28.27	23.04
Middle trunk of the brachial plexus		19.16	11.78	11.00	13.98
Lower trunk of the brachial plexus		35.82	16.49	28.27	26.86
Suprascapular nerve		3.14	3.53	3.53	3.40
Upper anterior division of brachial plexus		4.71	6.28	9.82	6.94
Upper posterior division of brachial plexus		4.12	12.37	15.71	10.73
Middle anterior division of brachial plexus		5.31	6.48	7.85	6.55
Middle posterior division of brachial plexus		6.54	7.85	5.89	6.76
Lower anterior division of brachial plexus		8.83	8.64	16.49	11.32
Lower posterior division of brachial plexus		7.20	8.64		7.92
Lateral cord of the brachial plexus	18.85	24.74	11.78	18.85	18.56
Medial cord of the brachial plexus	30.24	14.14	19.24	15.32	19.73
Posterior cord of the brachial plexus	29.85	21.99		43.98	31.94
Lateral pectoral nerve					
Medial pectoral nerve					
Medial brachial cutaneous nerve	4.71	3.53		2.36	3.53
Medial antebrachial cutaneous nerve	3.53				3.53
Thoracodorsal nerve		1.57	1.57	3.14	2.09
Subscapular nerve	2.36	1.57			1.96
Musculocutaneous nerve (in axilla/arm)	3.53	3.53	3.53	3.53	3.53
Lateral antebrachial cutaneous nerve	2.36	1.18		1.57	1.70
Lateral head of the median nerve	7.85	16.49	4.32	6.28	8.74
Medial head of the median nerve	6.28	3.93	4.71	6.28	5.30
Median nerve (in axilla/arm)	7.85	6.28	9.82	12.96	9.23
Anterior interosseous nerve		1.57			1.57
Median nerve (in forearm)	7.07	5.50			6.28
Palmar cutaneous branch of the median nerve		0.79			0.79
Median nerve (in carpal tunnel)		4.71			4.71
Palmar digital branches of the median nerve		4.71			4.71
Ulnar nerve (in axilla/arm)	7.85	5.50	5.50	6.28	6.28
Ulnar nerve (in forearm)	3.53	6.28		6.28	5.37
Cutaneous branch of the ulnar nerve		1.96			1.96
Deep branch of the ulnar nerve		1.96			1.96
Axillary nerve	7.85	9.42		4.71	7.33
Upper lateral brachial cutaneous nerve	1.57				1.57
Radial nerve (in axilla)	13.74	14.14		18.85	15.58
Nerve to triceps	2.36	1.57			1.96
Lower lateral brachial cutaneous nerve					
Posterior brachial cutaneous nerve		1.57			1.57
Posterior antebrachial cutaneous nerve					
Radial nerve (in arm)	10.60	6.28	7.07		7.98
Posterior interosseous nerve		2.36			2.36
Radial nerve (in forearm)	1.96	2.36			2.16

Table 5: Comparison of reported minimum and maximum total cross-sectional areas (mm^2) in 26 specimens [Sun61], and comparison with our estimates.

Nerve	Minimum Area	Maximum Area	Our Estimate
Medial brachial cutaneous nerve	0.39	3.93	3.53
Medial antebrachial cutaneous nerve	1.57	3.14	3.53
Lateral antebrachial cutaneous nerve	1.57	1.57	1.70
Radial nerve (in forearm)	1.18	3.93	2.16

Table 6: Comparison of predicted and measured cross-sectional areas (mm^2) of neural tissue. The measured areas are the same as those in the column labelled 'Average' in Table 4, but divided by 3 in order to convert total areas to neural areas.. The data are displayed graphically in Figure 1 on Page 11.

Nerve	Model Prediction	Slingluff et al	Our Data
C4 root	0.29		
C5 root	3.74	3.80	1.83
C6 root	6.61	6.79	3.14
C7 root	6.90	6.89	
C8 root	6.61	6.74	
T1 root	4.31	4.33	
T2 root	0.29	0.19	
Dorsal scapular nerve	0.37	0.35	
Long thoracic nerve	0.82	0.83	0.85
T1 pre-ganglionic sympathetic nerve	1.60		
Upper trunk of the brachial plexus	9.22	9.55	7.68
Middle trunk of the brachial plexus	6.83	6.85	4.66
Lower trunk of the brachial plexus	9.33	10.44	8.95
Suprascapular nerve	1.26	1.25	1.13
Upper anterior division of brachial plexus	4.48		2.31
Upper posterior division of brachial plexus	3.49		3.58
Middle anterior division of brachial plexus	2.73		2.39
Middle posterior division of brachial plexus	4.10		2.29
Lower anterior division of brachial plexus	7.34		4.36
Lower posterior division of brachial plexus	1.98		3.73
Lateral cord of the brachial plexus	7.21	6.97	6.19
Medial cord of the brachial plexus	7.34	7.37	6.58
Posterior cord of the brachial plexus	9.57	9.47	10.65
Lateral pectoral nerve	1.19	1.20	
Medial pectoral nerve	0.37	0.37	
Medial brachial cutaneous nerve	0.19	0.19	1.18
Medial antebrachial cutaneous nerve	1.06	1.04	1.18
Thoracodorsal nerve	0.59	0.60	0.70
Subscapular nerve	1.10	1.07	0.65
Musculocutaneous nerve (in axilla/arm)	1.98	1.91	1.18
Lateral antebrachial cutaneous nerve	0.06		0.57
Lateral head of the median nerve	4.01		2.91
Medial head of the median nerve	1.92		1.77
Median nerve (in axilla/arm)	5.93	5.86	3.08
Anterior interosseous nerve	0.74		0.52
Median nerve (in forearm)	4.69		2.09
Palmar cutaneous branch of the median nerve	1.95		0.26
Median nerve (in carpal tunnel)	2.74		1.57
Palmar digital branches of the median nerve	1.95		1.57
Ulnar nerve (in axilla/arm)	3.83	3.77	2.09
Ulnar nerve (in forearm)	3.17		1.79
Cutaneous branch of the ulnar nerve	2.08		0.65
Deep branch of the ulnar nerve	1.09		0.65
Axillary nerve	2.27	2.22	2.44
Upper lateral brachial cutaneous nerve	0.41	0.42	0.52
Radial nerve (in axilla)	5.62	5.54	5.19
Nerve to triceps	1.86		0.65
Lower lateral brachial cutaneous nerve	0.06		
Posterior brachial cutaneous nerve	0.63		0.52
Posterior antebrachial cutaneous nerve	0.63		
Radial nerve (in arm)	2.44		2.66
Posterior interosseous nerve	1.03		0.79
Radial nerve (in forearm)	0.70		0.72

Table 7: Comparison of predictions and observations of the proportions of cross-sectional area comprised of cutaneous fibres in three nerves. The observations are reproduced from Table 2.

Nerve	Model Prediction	Sunderland and Bedbrook
Radial nerve (in arm)	0.2865	0.2891
Median nerve (in axilla/arm)	0.6579	0.6710
Ulnar nerve (in axilla/arm)	0.5434	0.5442

Table 8: Comparison of predicted and standard myotomes. Each column shows the predicted proportion of each end-organs supply from the respective root. The standard root supply is indicated by the symbols '+' and '−', indicating a minor and a major contribution, respectively, from the root.

End-Organ	C5	C6	C7	C8	T1
Dilator pupillae					1.00 +
Rhomboids	1.00 +				
Supraspinatus	0.60 +	0.40 −			
Infraspinatus	0.60 +	0.40 −			
Latissimus dorsi		0.08 +	0.49 +	0.43 −	
Subscapularis	0.10 −	0.09 +	0.81 −		
Teres major		0.10 +	0.90 −		
Teres minor	0.66 +	0.34 −			
Serratus anterior	0.60 −	0.32 +	0.08 +		
Pectoralis major	0.04 −	0.03 −	0.69 +	0.15 +	0.09 −
Deltoid	0.67 +	0.33 −			
Coracobrachialis	0.03 −	0.03 +	0.93 −		
Biceps brachii	0.50 −	0.50 +			
Brachialis	0.27 −	0.26 +	0.47 −		
Triceps		0.03 −	0.34 +	0.63 +	
Anconeus			1.00 +		
Pronator teres		0.85 −	0.15 +		
Flexor carpi radialis		0.85 −	0.15 +		
Palmaris longus			0.05 +	0.95 +	
Flexor digitorum superficialis			0.03 −	0.56 +	0.42 −
Flexor carpi ulnaris			0.10 −	0.90 +	
Flexor digitorum profundus II + III				0.58 +	0.42 −
Flexor digitorum profundus IV + V				0.64 +	0.36 −
Flexor pollicis longus				0.58 +	0.42 −
Pronator quadratus				0.58 +	0.42 −
Brachioradialis	0.24 −	0.22 +	0.54 −		
Extensor carpi radialis longus		0.30 +	0.70 +		
Extensor carpi radialis brevis			0.51 +	0.49 −	
Extensor digitorum			0.52 +	0.48 −	
Extensor carpi ulnaris			0.52 −	0.48 +	
Supinator	0.52 −	0.48 +			
Extensor pollicis longus			0.52 −	0.48 +	
Extensor pollicis brevis			0.52 −	0.48 +	
Abductor pollicis longus			0.52 −	0.48 +	
Abductor pollicis brevis				0.59 +	0.41 −
Flexor pollicis brevis				0.51 +	0.49 −
Opponens pollicis				0.59 +	0.41 −
Adductor pollicis				0.51 −	0.49 +
Dorsal interossei				0.65 −	0.35 +
Palmar interossei				0.65 −	0.35 +

Acknowledgements

I am grateful to John Rollett for his advice on least-squares optimization techniques, to Tim Horder and Peter Burge for their help in obtaining anatomical data, and to Tony Hoare and Richard Stamper for their helpful comments on earlier drafts of this paper.

This work has been supported by an SERC Advanced Fellowship in Information Technology (SERC B/ITF/269), and an SERC Research Grant (SERC GR/F47077).

Author's Address

B.S. Todd FRCS, The Programming Research Group, Oxford University Computing Laboratory, 11 Keble Road, Oxford OX1 3QD, UK. (email Bryan.Todd@comlab.ox.ac.uk)

References

[And91] **Andreassen S, Jensen FV, Olesen KG**. Medical expert systems based on causal probabilistic networks. *International Journal of Biomedical Computing* (1991) **28** *i* 1-30.

[Bur91] **Burge P and Todd BS**. Computer-aided localization of peripheral nerve lesions. *Journal of Hand Surgery* (1991) **16-B** *i* 19-24.

[Cat79] **Catanzarite VA and Greenburg AG**. "Neurologist": a computer program for diagnosis in neurology. *Proceedings of the* 3rd *Annual Symposium on Computer Applications in Medical Care.* (1979) 64-71.

[Fir82] **First MB, Weimer BJ, McLinden S and Miller RA**. LOCALIZE: computer-assisted localization of peripheral nervous system lesions. *Computers and Biomedical Research* (1982) **15** 525-43.

[Fis90] **Fisher WS.** Computer-aided intelligence: application of an expert system to brachial plexus injuries. *Neurosurgery* (1990) **27** *v* 837-43.

[Hai88] **Hains G and Todd BS**. The parallel implementation of a medical diagnostic model. *Proceedings of the Third International Conference on Supercomputing* (1988) *i* 222-9.

[Har39] **Harris W**. *The Morphology of the Brachial Plexus.* Oxford University Press: London (1939), p85.

[Jas87] **Jaspers RBM and van der Helm, FCT**. Computer-aided diagnosis and treatment of brachial plexus injuries. *Lecture Notes in Medical Informatics* (1987) **33** 237-46.

[Jas90] **Jaspers RBM**. *Medical Decision Support: An Approach in the Domain of Brachial Plexus Injuries.* Thesis, Delft University of Technology (1990).

[Ker18] **Kerr AT**. Brachial plexus of nerves in man, the variations in its formation and branches. *American Journal of Anatomy* (1918) **23** *ii* 285-395.

[MRC76] **Medical Research Council**. *Aids to the Examination of the Peripheral Nervous System.* Her Majesty's Stationary Office: London (1976) Memorandum No. 45.

[Mil87] **Miller JD**. Clinical evaluation of the brachial plexus: a simplified approach. *Journal of the Missisipi State Medical Association* (1987) **28** 141-3.

[Nar78] **Narakas A**. Surgical treatment of traction injuries of the brachial plexus. *Clinical Orthopedics and Related Research* (1978) **133** 71-90.

[Nar81] **Narakas A**. Brachial plexus surgery. *Orthopedic Clinics of North America* (1981) **12** *ii* 303-23.

[Nea89] **Neapolitan RE**. *Probabilistic Reasoning in Expert Systems.* John Wiley: New York, Chichester (1989).

[Reg78] **Reggia JA**. A production rule system for neurological localization. *Proceedings of the* 2nd *Annual Symposium on Computer Applications in Medical Care.* (1978) 254-60.

[Sli87] **Slingluff CL, Terzis JK, Edgerton MT**. The quantitative microanatomy of the brachial plexus in man: reconstructive relevance. In **Terzis JK**, *Microreconstruction of Nerve Injuries.* WB Saunders: Philadelphia, London *etc.* (1987) *xxii* 285-324.

[Spi88] **Spivey JM**. *The Z Notation : A Reference Manual.* Prentice-Hall: Hemel Hempstead (1988).

[Spi89] **Spitzer K, Stein V, Thie A and Kunze K**. NERVTRACK - A neuroanatomical data bank. *Computers and Biomedical Research* (1989) **22** 181-9.

[Sun49] **Sunderland Sir S, Bedbrook GM**. The cross-sectional area of peripheral nerve trunks occupied by the fibres representing individual muscular nad cutaneous branches. *Brain* (1949) **72** 613-24.

[Sun61] **Sunderland Sir S, Bradley KC**. Stress-strain phenomena in human peripheral nerve trunks. *Brain* (1961) **84** 102-119.

[Sun78] **Sunderland Sir S**. *Nerves and Nerve Injuries.* 2nd edn. Churchill Livingstone: Edinburgh (1978).

[Swa86] **Swash M**. Diagnosis of brachial root and plexus lesions. *Journal of Neurology* (1986) **233** 131-5.

[Tod87] **Todd BS**. A model-based diagnostic program. *Software Engineering Journal* (1987) *May* 54-63.

[Tod88] **Todd BS**. *A Formal Approach to the Design of Medical Diagnostic Programs.* D.Phil. Thesis, Oxford University (1988).

[Tod90] **Todd BS**. An algorithm for approximating conditional probabilities. *International Journal of Bio-Medical Computing* (1990) **26** 29-38.